

Fermi surface origin of the interrelation between magnetocrystalline anisotropy and compositional order in transition metal alloys

S.S.A. Razee and J.B. Staunton

Department of Physics, University of Warwick, Coventry CV4 7AL, United Kingdom

B. Ginatempo and E. Bruno

Dipartimento di Fisica and Unità INFM, Università di Messina, Salita Sperone 31, I-98166 Messina, Italy

F.J. Pinski

Department of Physics, University of Cincinnati, Ohio 45221, USA

(February 6, 2008)

Recently, we outlined a scheme to investigate the effects of compositional order on the magnetocrystalline anisotropy of alloys from a first-principles electronic structure point of view {Phys. Rev. Lett. **83**, 5369 (1999)} and showed that compositional order enhances the magnitude of magnetocrystalline anisotropy energy (MAE) of $\text{Co}_{0.5}\text{Pt}_{0.5}$ alloy by some two orders of magnitude as well as affecting the equilibrium magnetization direction. Here we describe our scheme in detail and present an in-depth study of the effect by demonstrating its Fermi surface origin. In $\text{Co}_{0.25}\text{Pt}_{0.75}$ alloy we find that the perfect $L1_2$ structure has a very small MAE whereas imposition of directional order enhances the MAE by two orders of magnitude. We also present the effect of lattice distortion (tetragonalization) on the MAE on the same footing and find that in the $\text{Co}_{0.5}\text{Pt}_{0.5}$ alloy it accounts for only about 20% of the observed MAE, thus confirming that compositional order is the major player in the enhancement of MAE. We also examine the directional chemical order that can be produced by magnetic annealing within the same framework. We extract a Fermi surface mechanism for the effect in an explicit study of permalloy. Finally, we propose that the Fermi surface plays a major role in the strong coupling between magnetocrystalline anisotropy and compositional order in many magnetic alloys.

PACS numbers: 75.30.Gw, 75.50.Cc, 75.60.Nt, 75.50.Ss

I. INTRODUCTION

In recent years, there has been intensive theoretical as well as experimental research on the magnetocrystalline anisotropy of ferromagnetic materials containing transition metals, in particular, in the form of multilayers and thin films, because of the technological implications for high-density magneto-optical storage media.^{1–4} Areal densities of information storage systems are increasing continuously and are expected to reach 40 Gbits per square inch by the year 2004 which requires the grain size to be less than 10 nm. For such applications the films and multilayers need to exhibit a very strong perpendicular magnetic anisotropy^{5,6} (PMA) to avoid destabilization of the magnetization of recording bits by thermal fluctuations and demagnetizing fields.⁷ Whereas in ultrathin films and multilayers the PMA is due to surface^{8,9} and interface^{10,11} effects respectively, in thicker films of transition metal alloys it is the strong intrinsic bulk magnetocrystalline anisotropy which leads to PMA. Thick films of transition metal alloys are particularly interesting for magneto-optic recording because in addition to the required magneto-optic properties these are chemically stable and easy to manufacture. To design magnetic materials for future magneto-optic recording applications a detailed understanding of the mechanism of magnetocrystalline anisotropy is needed. A significant effort has been directed towards an understanding of the mi-

croscopic mechanism of magnetocrystalline anisotropy of these systems from a first-principles electronic structure point of view but since magnetocrystalline anisotropy arises from spin-orbit coupling, which is essentially a relativistic effect^{12,13} this means that a fully relativistic electronic structure framework is desirable.

Several experimental observations indicate a correlation between the compositional order and the magnetocrystalline anisotropy of ferromagnetic alloys, both in the bulk^{14–21} as well as in films.^{22–34} Very recently,³⁵ we developed a ‘first-principles’ theory of the interrelationship between the magnetocrystalline anisotropy and compositional order, both short- and long-ranged. In this theory the electronic structure is treated within the spin-polarized fully relativistic Korringa-Kohn-Rostoker coherent-potential approximation³⁶ (SPR-KKR-CPA) and the compositional order is modeled using the framework of static concentration waves³⁷ and is an extension of our earlier works^{38,39} on the magnetocrystalline anisotropy of disordered alloys. Within this scheme we showed for the first time that in fcc- $\text{Co}_{0.5}\text{Pt}_{0.5}$ alloy compositional order indeed has a profound influence on the magnetocrystalline anisotropy, especially in the way it breaks cubic symmetry. In this paper, we describe our scheme in some detail and provide an in-depth study of this effect in another CoPt alloy and demonstrate an electronic origin of the enhancement of the magnetocrystalline anisotropy energy (MAE). Also, it is known exper-

imentally that, upon ordering, the equiatomic CoPt alloy undergoes a modest tetragonal lattice distortion ($c/a = 0.98$) which can also enhance the MAE. We have calculated the MAE of disordered fcc-Co_{0.5}Pt_{0.5} alloy for different c/a ratios and find that a 2% tetragonalization would contribute only about 20% of the observed MAE. This is a clear indication that in CoPt system, the enhancement of MAE is primarily due to compositional order. This inference gets further credence from the fact that fcc-Co_{0.25}Pt_{0.75} alloy, which retains its cubic lattice structure upon ordering, also shows an enhancement of MAE when compositional order is introduced.

We have studied the effects of compositional modulation on the MAE of fcc-Co_cPt_{1-c} for $c=0.25$ and 0.5 alloys. Thick films of these alloys are potential magneto-optical recording materials because they exhibit large perpendicular anisotropy,^{22–26,40} large magneto-optic Kerr effect signals compared to the Co/Pt multilayers and the currently used TbFeCo films for a large range of wavelengths^{22,23} (400–820 nm), have suitable Curie temperatures⁴¹ (~ 700 K), high oxidation and corrosion resistance as well as being chemically stable and easy to manufacture. We investigate the observed ordered structures as well as some hitherto unfabricated structures of these alloys with same stoichiometry. This is pertinent now that it is possible to *tailor* compositionally modulated films to obtain better magneto-optic recording characteristics.^{42,43} We find that, compositional ordering enhances the size of MAE by some two orders of magnitude for all the compositions in addition to altering the magnetic easy axis in some cases. The easy axis in all the layered-ordered structures lies perpendicular to the layer-stacking. Of particular interest is the case of Co_{0.25}Pt_{0.75}. MAE for the perfect $L1_2$ ordered alloy is very small as in the homogeneously disordered alloy with the easy axis along the [111] direction. However, breaking this symmetry by some kind of a directional chemical order and creating *internal interfaces* enhances the MAE by two orders of magnitude as well as making the easy axis perpendicular to the interfaces, in excellent agreement with the experimental observations.³² By analyzing the electronic structure of these alloys we find that the electrons near the Fermi surface, in particular, those electrons around the X-points in the Brillouin zone, are largely responsible for the enhancement of MAE by compositional ordering.

Using the same theoretical framework, we have also studied the phenomenon of magnetic annealing in Ni_{0.75}Fe_{0.25} permalloy, which develops uniaxial magnetic anisotropy when annealed in a magnetic field.^{20,21} Because of its high permeability and low coercivity, the permalloy is a good soft magnet and can be used for low switching fields in sensors. Also, a large difference in the conductivity of majority and minority spins⁴⁴ makes it a good candidate for spin-valves, spin transistors and magnetic tunnel junctions. On magnetic annealing, the permalloy develops directional chemical order^{45,46} which is responsible for the uniaxial anisotropy. In the previous

work³⁵ we showed for the first time from first-principles theoretical calculations that magnetic annealing can indeed produce directional chemical order. Here we isolate the electronic origin of the effect.

The outline of the paper is as follows. In Sec. II, we present the formulation. In Sec. III we provide some numerical and technical details. Afterwards, we present our results in Sec. IV and in Sec. V we investigate the electronic origin of the MAE enhancement as well as of the magnetic annealing. Finally, in Sec. VI we draw some conclusions.

II. FORMULATION

Our theory is based on the relativistic spin-polarized local density functional theory^{47–49} and its solution by the SPR-KKR-CPA method.^{36,50} A detailed description of the method for the homogeneously disordered ferromagnetic alloys is provided in Ref. 38, and will not be repeated. Here, we describe in detail our new framework to investigate the effects of compositional order, both short- and long-ranged, on the magnetocrystalline anisotropy (A summary of the approach has already been described in our recent letter Ref. 35). In Sec. II A we give a brief outline of the theory of compositional order within the SPR-KKR-CPA formalism and in Sec. II B we describe the scheme for studying the effects of compositional order on the MAE together with the theory of magnetic annealing. Also, in this section we describe a scheme to investigate the electronic origin of the enhancement of MAE upon ordering.

A. Compositional order

We consider a binary alloy A_cB_{1-c} where the atoms are arranged on a fairly regular array of lattice sites. At high temperatures the alloy is homogeneously disordered and each site is occupied by an A - or B -type atom with probabilities c and $(1-c)$ respectively. Below some transition temperature, T_c , the system will either order or phase separate. A compositionally modulated alloy can be described by a set of site-occupation variables $\{\xi_i\}$, with $\xi_i = 1(0)$ when the i -th site in the lattice is occupied by an $A(B)$ -type atom. The thermodynamic average, $\langle \xi_i \rangle$, of the site-occupation variable is the concentration c_i of an A -type atom at that site. At high temperatures where the alloy is homogeneously disordered, $c_i = c$ for all sites. When inhomogeneity sets in below T_c , the temperature-dependent inhomogeneous concentration fluctuations $\{\delta c_i\} = \{c_i - c\}$ can be written as a superposition of static concentration waves,³⁷ i.e.,

$$c_i = c + \frac{1}{2} \sum_{\mathbf{q}} [c_{\mathbf{q}} e^{i\mathbf{q} \cdot \mathbf{R}_i} + c_{\mathbf{q}}^* e^{-i\mathbf{q} \cdot \mathbf{R}_i}],$$

where, $c_{\mathbf{q}}$ are the amplitudes of the concentration waves with wave-vectors \mathbf{q} , and \mathbf{R}_i are the lattice positions. Usually only a few concentration waves are needed to describe a particular ordered structure. For example, the CuAu-like $L1_0$ layered-ordered structure (Fig. 1) is set up by a single concentration wave with $c_{\mathbf{q}} = \frac{1}{2}$ and $\mathbf{q} = (001)$, the [111]-layered CuPt-like $L1_1$ ordered structure is set up by a concentration wave with $c_{\mathbf{q}} = \frac{1}{2}$ and $\mathbf{q} = (\frac{1}{2} \frac{1}{2} \frac{1}{2})$, and the Cu₃Au-like $L1_2$ ordered structure is set up by three concentration waves of identical amplitude $c_{\mathbf{q}} = \frac{1}{4}$ and wave-vectors $\mathbf{q}_1 = (100)$, $\mathbf{q}_2 = (010)$, and $\mathbf{q}_3 = (001)$ (\mathbf{q} is in units of $\frac{2\pi}{a}$, a being the lattice parameter).

The grand-potential for the interacting electrons in an inhomogeneous alloy with composition $\{c_i\}$ and magnetized along the direction \mathbf{e} at a finite temperature T is given by,^{51–53}

$$\Omega(\{c_i\}; \mathbf{e}) = \nu Z - \int_{-\infty}^{\infty} d\varepsilon f(\varepsilon, \nu) N(\{c_i\}, \varepsilon; \mathbf{e}) + \Omega_{DC}(\{c_i\}; \mathbf{e}), \quad (2.1)$$

where, ν is the chemical potential, Z is the total valence charge, $f(\varepsilon, \nu)$ is the Fermi factor, $N(\{c_i\}, \varepsilon; \mathbf{e})$ is the integrated electronic density of states, and $\Omega_{DC}(\{c_i\}; \mathbf{e})$ is the ‘double-counting’ correction to the grand-potential.⁵² The derivatives of the grand potential with respect to the concentration variables give rise to a hierarchy of direct correlation functions. In particular, the second derivative evaluated at the equilibrium concentrations,

$$S_{jk}^{(2)}(\mathbf{e}) = \left. \frac{\partial^2 \Omega(\{c_i\}; \mathbf{e})}{\partial c_j \partial c_k} \right|_{\{c_i=c\}},$$

is the Ornstein-Zernike direct correlation function for our lattice model^{51–55} (so called by the way of the close analogy with similar quantities defined for classical fluids^{56,57}). These are related to the linear response functions, $\alpha_{ij}(\mathbf{e})$, through⁵³

$$\left[1 + \sum_k S_{ik}^{(2)}(\mathbf{e}) \alpha_{ki}(\mathbf{e}) \right] \alpha_{ij}(\mathbf{e}) = \beta c(1-c) \left[\delta_{ij} + \sum_k S_{ik}^{(2)}(\mathbf{e}) \alpha_{kj}(\mathbf{e}) \right], \quad (2.2)$$

where $\beta = (k_B T)^{-1}$, k_B being the Boltzmann constant. The linear response functions, $\alpha_{ij}(\mathbf{e})$, describe the resulting concentration fluctuations, $\{\delta c_i\}$, which are produced when a small inhomogeneous set of external chemical potentials, $\{\delta \nu_i\}$, is applied at all sites. Via the fluctuation dissipation theorem these are proportional to atomic pair-correlation functions, i.e. $\alpha_{ij} = \beta[\langle \xi_i \xi_j \rangle - \langle \xi_i \rangle \langle \xi_j \rangle]$. Upon taking the lattice Fourier transform of Eq. (2.2) we obtain a closed form of equations,^{51–55}

$$\alpha(\mathbf{q}, T; \mathbf{e}) = \frac{\beta c(1-c)}{1 - \beta c(1-c)[S^{(2)}(\mathbf{q}; \mathbf{e}) - \lambda_c]}, \quad (2.3)$$

where, the Onsager cavity correction λ_c is given by,⁵³

$$\lambda_c = \frac{1}{\beta c(1-c)} \frac{1}{V_{BZ}} \int d\mathbf{q}' S^{(2)}(\mathbf{q}'; \mathbf{e}) \alpha(\mathbf{q}', T; \mathbf{e}).$$

Here, $\alpha(\mathbf{q}, T)$, the lattice Fourier transform of α_{ij} , are the Warren-Cowley atomic short-range order (ASRO) parameters in the disordered phase. The Onsager cavity correction in Eq. (2.3) ensures that the spectral weight over the Brillouin zone is conserved,^{53,55,58} so that, in other words, the diagonal part of the fluctuation dissipation theorem is honored, i.e. $\alpha_{ii} = \beta c(1-c)$.

The spinodal transition temperature T_c below which the alloy orders into a structure characterized by the concentration wave-vector \mathbf{q}_{max} is determined by $S^{(2)}(\mathbf{q}_{max}; \mathbf{e})$, where \mathbf{q}_{max} is the value at which $S^{(2)}(\mathbf{q}; \mathbf{e})$ is maximal. Neglecting the Onsager cavity correction, we can write,^{51,52}

$$T_c = \frac{c(1-c)S^{(2)}(\mathbf{q}_{max}; \mathbf{e})}{k_B}.$$

For the purpose of this study, we need only to consider the effects of compositional fluctuations in which charge rearrangement effects are neglected. Within the SPR-KKR-CPA scheme, a formula for $S_{jk}^{(2)}(\mathbf{e})$ is obtained by using Lloyd formula⁵⁹ for the integrated density of states in Eq. (2.1),

$$S_{jk}^{(2)}(\mathbf{e}) = - \frac{Im}{\pi} \int_{-\infty}^{\infty} d\varepsilon f(\varepsilon, \nu) Tr \left[\{ X^A(\mathbf{e}) - X^B(\mathbf{e}) \} \times \sum_{m \neq j} \tau^{jm}(\mathbf{e}) \Lambda^{mk}(\mathbf{e}) \tau^{mj}(\mathbf{e}) \right], \quad (2.4)$$

where,

$$X^{A(B)}(\mathbf{e}) = \left[\left\{ t_{A(B)}^{-1}(\mathbf{e}) - t_c^{-1}(\mathbf{e}) \right\}^{-1} + \tau^{00}(\mathbf{e}) \right]^{-1},$$

and

$$\Lambda^{jk}(\mathbf{e}) = \delta_{jk} \{ X^A(\mathbf{e}) - X^B(\mathbf{e}) \} - X^A(\mathbf{e}) \sum_{m \neq j} \tau^{jm}(\mathbf{e}) \Lambda^{mk}(\mathbf{e}) \tau^{mj}(\mathbf{e}) X^B(\mathbf{e}).$$

Here $t_{A(B)}(\mathbf{e})$ and $t_c(\mathbf{e})$ are the t-matrices for electronic scattering from sites occupied by $A(B)$ atoms and CPA effective potentials respectively, and $\tau^{mj}(\mathbf{e})$ are the path operator matrices for the CPA effective medium in real space obtained by a lattice Fourier transform of $\tau(\mathbf{k}; \mathbf{e})$, where

$$\tau(\mathbf{k}; \mathbf{e}) = [t_c^{-1}(\mathbf{e}) - g(\mathbf{k})]^{-1},$$

$g(\mathbf{k})$ being the KKR structure constants matrix.⁶⁰ Now taking the lattice Fourier transform of Eq. (2.4), we get

$$S^{(2)}(\mathbf{q}; \mathbf{e}) = -\frac{Im}{\pi} \int_{-\infty}^{\infty} d\varepsilon f(\varepsilon, \nu) \times \sum_{L_1 L_2 L_3 L_4} \left[\{X^A(\mathbf{e}) - X^B(\mathbf{e})\}_{L_1 L_2} \times I_{L_2 L_3; L_4 L_1}(\mathbf{q}; \mathbf{e}) \Lambda_{L_3 L_4}(\mathbf{q}; \mathbf{e}) \right], \quad (2.5)$$

where,

$$\begin{aligned} \Lambda_{L_1 L_2}(\mathbf{q}; \mathbf{e}) &= \{X^A(\mathbf{e}) - X^B(\mathbf{e})\}_{L_1 L_2} \\ &- \sum_{L_3 L_4 L_5 L_6} \left[X_{L_1 L_5}^A(\mathbf{e}) I_{L_5 L_3; L_4 L_6}(\mathbf{q}; \mathbf{e}) \times X_{L_6 L_2}^B(\mathbf{e}) \Lambda_{L_3 L_4}(\mathbf{q}; \mathbf{e}) \right], \end{aligned}$$

and,

$$I_{L_5 L_3; L_4 L_6}(\mathbf{q}; \mathbf{e}) = \frac{1}{V_{BZ}} \int d\mathbf{k} \tau_{L_5 L_3}(\mathbf{k} + \mathbf{q}; \mathbf{e}) \tau_{L_4 L_6}(\mathbf{k}; \mathbf{e}) - \tau_{L_5 L_3}^{00}(\mathbf{e}) \tau_{L_4 L_6}^{00}(\mathbf{e}). \quad (2.6)$$

Experimentally, the instability of the disordered phase to ordering can be observed in diffuse electron, x-ray, or neutron scattering experiments. The experimentally measured intensities are proportional to the ASRO parameter. In previous works, the ASRO parameter $\alpha(\mathbf{q}, T)$ and ordering temperature T_c have been calculated for many alloys, both non-magnetic and ferromagnetic, and were compared with diffuse x-ray and neutron scattering data.^{52,53} However, in those studies, relativistic effects were largely ignored. These studies have revealed that the electronic structure around the Fermi level is sometimes the driving force behind unusual compositional ordering in some alloys.^{51,53} Schematically, $S^{(2)}(\mathbf{q}; \mathbf{e})$ can be written in terms of the convolution of Bloch spectral density functions⁶⁰ $A_B(\mathbf{k}, \varepsilon; \mathbf{e})$ as,⁵¹

$$S^{(2)}(\mathbf{q}; \mathbf{e}) \sim \int_{-\infty}^{\infty} d\varepsilon \int_{-\infty}^{\infty} d\varepsilon' \frac{f(\varepsilon, \nu) - f(\varepsilon', \nu)}{\varepsilon - \varepsilon'} \times \int d\mathbf{k} A_B(\mathbf{k} + \mathbf{q}, \varepsilon; \mathbf{e}) A_B(\mathbf{k}, \varepsilon'; \mathbf{e}). \quad (2.7)$$

For perfectly ordered alloys, this reduces to a standard susceptibility form.⁵² In some cases the principal contribution to $S^{(2)}(\mathbf{q}; \mathbf{e})$ comes from energies close to the Fermi level ν . Thus $S^{(2)}(\mathbf{q}; \mathbf{e})$ can be large around the Fermi energy in two ways. In the conventional Fermi surface ‘nesting’ mechanism^{51,52} overlap takes place over extended regions of the reciprocal space between almost parallel flat sheets of Fermi surface⁵¹ with spanning vector \mathbf{Q} as in $\text{Cu}_{0.75}\text{Pd}_{0.25}$. The structures based on this mechanism will tend to be long period or incommensurate structures. Alternatively, a large $S^{(2)}(\mathbf{q}; \mathbf{e})$ can result from a spanning vector connecting the van Hove singularities around high-symmetry points,⁶¹ as in

$\text{Cu}_{0.5}\text{Pt}_{0.5}$. The structures based on this mechanism will tend to produce high symmetry structures with short periodicities since the spanning vector will be that which connects the high-symmetry points in the Brillouin zone. We find similar Fermi surface effects contribute to the enhancement of MAE by compositional order found in $\text{Co}_c\text{Pt}_{1-c}$ alloys, and propose that the mechanism is widespread in other magnetic transition-metal alloys.

B. Magnetocrystalline Anisotropy

The MAE of the inhomogeneous alloy can be characterized by the change in the electronic grand-potential arising from the change in the magnetization direction. Thus,

$$K(\{c_i\}) = \Omega(\{c_i\}; \mathbf{e}_1) - \Omega(\{c_i\}; \mathbf{e}_2),$$

where, \mathbf{e}_1 and \mathbf{e}_2 are two magnetization directions. We assume that the double-counting correction $\Omega_{DC}(\{c_i\}; \mathbf{e})$ is generally unaffected by the change in the magnetization direction, and therefore, only the first two terms of Eq. (2.1) contribute to the MAE,

$$\begin{aligned} K(\{c_i\}) &= (\nu_1 - \nu_2) Z - \int_{-\infty}^{\infty} d\varepsilon f(\varepsilon, \nu_1) N(\{c_i\}, \varepsilon; \mathbf{e}_1) \\ &+ \int_{-\infty}^{\infty} d\varepsilon f(\varepsilon, \nu_2) N(\{c_i\}, \varepsilon; \mathbf{e}_2), \end{aligned}$$

where ν_1 and ν_2 are the chemical potentials of the system when the magnetization is along \mathbf{e}_1 and \mathbf{e}_2 directions respectively. The change in the chemical potential originates from a redistribution of the occupied energy bands in the Brillouin zone in the event of a change of magnetization direction. A Taylor expansion of $f(\varepsilon, \nu_2)$ about ν_1 and some algebra leads to,

$$\begin{aligned} K(\{c_i\}) &= \int_{-\infty}^{\infty} d\varepsilon f(\varepsilon, \nu_1) [N(\{c_i\}, \varepsilon; \mathbf{e}_1) - N(\{c_i\}, \varepsilon; \mathbf{e}_2)] \\ &+ O(\nu_1 - \nu_2)^2, \end{aligned}$$

Note that the effect of the small change in the chemical potential on $K(\{c_i\})$ is of second order in $(\nu_1 - \nu_2)$, and can be shown to be very small compared to the first term.³⁸ We now expand $K(\{c_i\})$ around $K_{CPA}(c)$, the MAE of the homogeneously disordered alloy $A_c B_{1-c}$,

$$\begin{aligned} K(\{c_i\}) &= K_{CPA}(c) + \sum_j \frac{\partial K(\{c_i\})}{\partial c_j} \Big|_{\{c_i=c\}} \delta c_j \\ &+ \frac{1}{2} \sum_{j,k} \frac{\partial^2 K(\{c_i\})}{\partial c_j \partial c_k} \Big|_{\{c_i=c\}} \delta c_j \delta c_k + O(\delta c)^3. \quad (2.8) \end{aligned}$$

It is clear from Eq. (2.8) that we are considering only the effects of two-site correlations on the electronic grand-potential and MAE. However, in principle it is possible to include higher order correlations, but computationally it will be prohibitive.

Within the SPR-KKR-CPA scheme, a formula for $K_{CPA}(c)$ is obtained by using the Lloyd formula⁵⁹ for the integrated density of states,

$$K_{CPA}(c) = -\frac{Im}{\pi} \int_{-\infty}^{\infty} d\varepsilon f(\varepsilon, \nu_1) \left[\frac{1}{V_{BZ}} \int d\mathbf{k} \right. \\ \times \ln \|I + \{t_c^{-1}(\mathbf{e}_2) - t_c^{-1}(\mathbf{e}_1)\} \tau(\mathbf{k}; \mathbf{e}_1)\| \\ + c \left(\ln \|D^A(\mathbf{e}_1)\| - \ln \|D^A(\mathbf{e}_2)\| \right) \\ + (1-c) \left(\ln \|D^B(\mathbf{e}_1)\| - \ln \|D^B(\mathbf{e}_2)\| \right) \\ \left. + \mathcal{O}(\nu_1 - \nu_2)^2 \right], \quad (2.9)$$

where

$$D^{A(B)}(\mathbf{e}) = \left[I + \tau^{00}(\mathbf{e}) \{t_{A(B)}^{-1}(\mathbf{e}) - t_c^{-1}(\mathbf{e})\} \right]^{-1}.$$

Note that Eq. (2.9) is the finite temperature version of the expression of MAE of disordered alloys given in Ref. 38. Now, the variation of the MAE with respect to the change in the concentration variables is,

$$\left. \frac{\partial K(\{c_i\})}{\partial c_j} \right|_{\{c_i=c\}} = -\frac{Im}{\pi} \int_{-\infty}^{\infty} d\varepsilon f(\varepsilon, \nu_1) \\ \times \left[\ln \|D^A(\mathbf{e}_1)\| - \ln \|D^B(\mathbf{e}_1)\| \right. \\ \left. - \ln \|D^A(\mathbf{e}_2)\| + \ln \|D^B(\mathbf{e}_2)\| \right],$$

which is independent of the site-index and so the second term in Eq. (2.8) vanishes if the number of A and B atoms in the alloy is to be conserved ($\sum_j \delta c_j = 0$). Also, we have,

$$\left. \frac{\partial^2 K(\{c_i\})}{\partial c_j \partial c_k} \right|_{\{c_i=c\}} = S_{jk}^{(2)}(\mathbf{e}_1) - S_{jk}^{(2)}(\mathbf{e}_2),$$

where, $S_{jk}^{(2)}(\mathbf{e}_{1(2)})$ are the Ornstein-Zernike direct correlation functions⁵¹ when the magnetization is along $\mathbf{e}_{1(2)}$. Now taking the Fourier transform of Eq. (2.8), we get the MAE of the compositionally modulated alloy with wave-vector \mathbf{q} ,

$$K(\mathbf{q}) = K_{CPA}(c) + \frac{1}{2} |c_{\mathbf{q}}|^2 K^{(2)}(\mathbf{q}), \quad (2.10)$$

where

$$K^{(2)}(\mathbf{q}) = S^{(2)}(\mathbf{q}; \mathbf{e}_1) - S^{(2)}(\mathbf{q}; \mathbf{e}_2). \quad (2.11)$$

Eq. (2.10) thus shows a direct relationship between the type of compositional modulation and the MAE. Also, by

calculating $S^{(2)}(\mathbf{q}; \mathbf{e})$ for different \mathbf{q} -vectors, while keeping the magnetic field and magnetization direction fixed, one can study the effect of an applied magnetic field on the compositional modulation of a solid solution, and thus can describe the phenomenon of magnetic annealing. In this case, the \mathbf{q} -vector for which $S^{(2)}(\mathbf{q}; \mathbf{e})$ is maximal will represent the compositional modulation induced in the alloy when it is annealed in the magnetic field.

In our previous studies on disordered alloys^{38,39} we have found that the MAE originates from the change in the electronic structure around the Fermi energy caused by altering the magnetization direction. The changed electronic structure around the Fermi surface caused by the compositional order is thus the reason for the enhancement of MAE in the ordered phase. To understand this effect we undertake the following analysis. Using the same argument leading to Eq. (2.7) we arrive at,

$$K^{(2)}(\mathbf{q}) \sim \int_{-\infty}^{\infty} d\varepsilon \int_{-\infty}^{\infty} d\varepsilon' \frac{f(\varepsilon, \nu) - f(\varepsilon', \nu)}{\varepsilon - \varepsilon'} \\ \times \int d\mathbf{k} [A_B(\mathbf{k} + \mathbf{q}, \varepsilon; \mathbf{e}_1) A_B(\mathbf{k}, \varepsilon'; \mathbf{e}_1) \\ - A_B(\mathbf{k} + \mathbf{q}, \varepsilon; \mathbf{e}_2) A_B(\mathbf{k}, \varepsilon'; \mathbf{e}_2)]$$

which can be rewritten as,

$$K^{(2)}(\mathbf{q}) \sim \frac{1}{2} \int_{-\infty}^{\infty} d\varepsilon \int_{-\infty}^{\infty} d\varepsilon' \frac{f(\varepsilon, \nu) - f(\varepsilon', \nu)}{\varepsilon - \varepsilon'} \\ \times \int d\mathbf{k} [\Sigma(\mathbf{k} + \mathbf{q}, \varepsilon) \Delta(\mathbf{k}, \varepsilon') \\ + \Sigma(\mathbf{k}, \varepsilon') \Delta(\mathbf{k} + \mathbf{q}, \varepsilon)] \quad (2.12)$$

where,

$$\Sigma(\mathbf{k}, \varepsilon) = A_B(\mathbf{k}, \varepsilon; \mathbf{e}_1) + A_B(\mathbf{k}, \varepsilon; \mathbf{e}_2) \quad (2.13)$$

and

$$\Delta(\mathbf{k}, \varepsilon) = A_B(\mathbf{k}, \varepsilon; \mathbf{e}_1) - A_B(\mathbf{k}, \varepsilon; \mathbf{e}_2). \quad (2.14)$$

The principal contributions to $K^{(2)}(\mathbf{q})$ will come from energies close to the Fermi energy ν . Thus, $K^{(2)}(\mathbf{q})$ will be large for \mathbf{q} -vectors corresponding to the spanning vectors $\mathbf{q} = \mathbf{Q}$ connecting the peaks in $\Sigma(\mathbf{k}, \varepsilon)$ and $\Delta(\mathbf{k}, \varepsilon)$ for ε close to the Fermi energy. Therefore, a close examination of $\Sigma(\mathbf{k}, \nu)$ and $\Delta(\mathbf{k}, \nu)$ will give an idea as to which composition modulations will produce a large MAE.

III. COMPUTATIONAL DETAILS

In this section we discuss the technical details in the calculation of MAE of compositionally modulated alloys. In a homogeneously disordered alloy, the MAE is of the order of μeV and the MAE of the ordered systems can

be as high as 0.5meV. But the MAE is still several orders of magnitude smaller than the band energies as well as the total energy. For this reason the calculation of MAE needs great care. In an earlier publication³⁸ we presented a robust scheme to calculate the MAE, where we proposed that one should calculate the difference in the total energies for the two magnetization directions directly rather than subtracting the two total energies calculated separately. We included a detailed discussion on the computational and technical aspects of solving the SPR-KKR-CPA equations as well as the calculation of MAE of the disordered alloys and do not repeat that discussion here. Instead, we will focus only on the calculation of $S^{(2)}(\mathbf{q}; \mathbf{e})$ and $K^{(2)}(\mathbf{q})$.

The integration over the energies involved in Eqs. (2.5) and (2.11) is carried out using a complex contour because in the complex plane, the integrand becomes a smooth function of both energy as well as \mathbf{k} and consequently we need fewer energy points as well as fewer \mathbf{k} -points to obtain an accurate integral.⁶² In our calculation, we have used a rectangular box contour as described in detail in Ref. 38.

The most demanding part of the whole calculation is the evaluation of the convolution $I(\mathbf{q}; \mathbf{e})$ given by Eq. (2.6). Owing to the form of the integrand the integration has to be done using the full Brillouin zone. We performed the Brillouin zone integration by using the adaptive grid method⁶³ which has been found to be very efficient and accurate. In this method one can preset the level of accuracy of the integration by supplying a tolerance parameter ϵ . The number of \mathbf{k} -points used in the integration thus depends directly on ϵ . In the present work, the integration in Eq. (2.6) is carried out with $\epsilon = 10^{-6}$ which means that values of $S^{(2)}(\mathbf{q}; \mathbf{e})$ which are of the order of 0.1 eV are accurate up to 0.1 μeV . To achieve such level of accuracy, we had to sample a large number of \mathbf{k} -points in the Brillouin zone. Typically, in our calculations, we needed around 35,000 \mathbf{k} -points in the full Brillouin zone for energies with an imaginary part of 0.5 Ry. When the energy was 0.0001 Ry above the real axis (and that is the closest point to the real axis, we need) we required as many as 3 million \mathbf{k} -points in the full Brillouin zone for the same level of accuracy. Furthermore, we have calculated $S^{(2)}(\mathbf{q}; \mathbf{e}_1)$ and $S^{(2)}(\mathbf{q}; \mathbf{e}_2)$ simultaneously ensuring that they are calculated on the same grid of \mathbf{k} -points, and thus cancelling out the systematic errors if there are any. Therefore, we claim that the values of $K(\mathbf{q})$ are accurate to within 0.1 μeV .

IV. RESULTS AND DISCUSSION

A. $\text{Co}_c\text{Pt}_{1-c}$ alloy

We have studied $\text{Co}_c\text{Pt}_{1-c}$ alloys for $c=0.5$ and 0.25. It is well known that disordered fcc- $\text{Co}_{0.5}\text{Pt}_{0.5}$ undergoes a phase transformation into a CuAu-type $L1_0$ or-

dered tetragonal structure^{14,64} with a c/a ratio of 0.98 below 1100 K, and $\text{Co}_{0.25}\text{Pt}_{0.75}$ orders into a Cu₃Au-type $L1_2$ cubic structure⁶⁵ below 960 K. Thus, in case of the equiatomic composition, the tetragonalization of the lattice which also lowers the symmetry could also be responsible for MAE enhancement, whereas in $\text{Co}_{0.25}\text{Pt}_{0.75}$ there is no such additional effect, because the lattice remains cubic even in the ordered phase. With this in mind we calculated the MAE of disordered volume-conserving face-centered-tetragonal $\text{Co}_{0.5}\text{Pt}_{0.5}$ alloy as a function of the c/a ratio. The results are presented in Fig. 2. We point out that in these calculations we have used atomic-sphere approximation for the single-site potentials and that the potentials and the Fermi energy are those of the disordered fcc- $\text{Co}_{0.5}\text{Pt}_{0.5}$ alloy. To estimate the magnitude of the effect of tetragonalization we have ‘frozen’ these potentials as the c/a ratio has been altered. We observe that the MAE is a monotonically decreasing function of the c/a ratio, and that it is positive for $c/a < 1.0$ and negative for $c/a > 1.0$. This is consistent with the experimental observations that the magnetostriction constant, λ_{001} , is positive^{31,66} for the disordered $\text{Co}_{0.5}\text{Pt}_{0.5}$ alloy. Because, Freeman *et al*⁶⁷ have shown that λ_{001} is proportional to the rate of change of MAE with respect to the c/a ratio, and that λ_{001} has the opposite sign to that of the later (Note that, there is a sign difference in our definition of MAE and that of Freeman *et al*). Therefore, our results are in qualitative agreement with the experimental observations. The MAE at the experimental value of c/a (0.98) is about 25 μeV which is less than 20% of the experimentally observed MAE. Most importantly, the sign of MAE for this value of c/a is positive which means that the magnetic easy axis is not along the [001] direction (c -axis) in direct contradiction to the experimental observations. Consequently, we conclude that in the ordered alloys of Co and Pt lattice distortion is not the major factor in determining the MAE rather it is the compositional order which is primarily responsible for the large MAE.

Now we present the effect of compositional order on the magnetocrystalline anisotropy. In our studies, we explore the observed equilibrium ordered structures as well as some hypothetical ordered structures of these alloys keeping the stoichiometry constant. The results are summarized in Tables I and II. First we discuss $\text{Co}_{0.5}\text{Pt}_{0.5}$. We note that, $S^{(2)}(\mathbf{q})$ is maximum for the $L1_0$ structure, implying that the alloy would order into this structure at 1360 K as it is cooled from high temperature in good agreement with experiment (experimental value of the ordering temperature is 1100 K). From Table II we note that for $\mathbf{q} = (001)$ and $\mathbf{q} = (100)$ which correspond to CuAu-like $L1_0$ ordered structure, with Co and Pt layers stacked along the [001] and [100] directions respectively, the direction of spontaneous magnetization is along the [001] and [100] directions respectively in excellent agreement with experiment. Also, the MAE (58.6 μeV) is comparable to the experimental value^{14–16} ($\sim 130\mu\text{eV}$) as well as to the calculated value of the $L1_0$ -ordered tetrag-

onal CoPt alloy.⁶⁸ In the CuPt-type $L1_1$ layered structure set up by $\mathbf{q} = (\frac{1}{2}\frac{1}{2}\frac{1}{2})$, the equilibrium direction of magnetization is along the [111] direction of the crystal, i.e. again perpendicular to the layer-stacking. The structure set up by concentration waves with $\mathbf{q} = (10\frac{1}{2})$ and $(01\frac{1}{2})$ is also a [001]-oriented layered structure, but the layers are not alternately pure Co and Pt planes, rather they are layers of CoPt in a particular order (Fig. 1). Even in this case, we note that the magnetization is perpendicular to the layered structure. Similarly, for $\mathbf{q} = (\frac{1}{2}01)$ and $(\frac{1}{2}10)$ where the planes are stacked along the [100] direction the magnetization is also along the [100] direction.

In case of $\text{Co}_{0.25}\text{Pt}_{0.75}$, $S^{(2)}(\mathbf{q})$ has a maxima for $\mathbf{q} = (100)$, (010) , and (001) implying that a $L1_2$ ordered structure is favored with a transition temperature of 935 K in excellent agreement with the experimental value of 960 K (Ref. 65). Note that, a combination of three wave-vectors $\mathbf{q}_1 = (100)$, $\mathbf{q}_2 = (010)$, and $\mathbf{q}_3 = (001)$ generates the isotropic $L1_2$ ordering, while a single wave-vector, for example, $\mathbf{q}_1 = (001)$ generates a layered structure with directional compositional ordering along the [001] direction. This is a superstructure consisting of alternating monolayers of pure Pt and $\text{Co}_{0.5}\text{Pt}_{0.5}$, as depicted in Fig. 1. In this structure, therefore, there are no out-of-plane Co-Co bonds, only in-plane Co-Co bonds which can produce only in-plane Co-Co nearest neighbor pairs. We find that for this structure, the easy axis is along the [001] direction, *i.e.* perpendicular to the layers, and the MAE is also quite large ($\sim 84 \mu\text{eV}$). In a recent experiment,²⁷ it was found that, the [001]-textured thick films of $\text{Co}_{0.25}\text{Pt}_{0.75}$ alloy deposited at 670 K do have this type of structure, *i.e.* there are stacks of Pt and $\text{Co}_{0.5}\text{Pt}_{0.5}$ monolayers perpendicular to the [001] direction, and these films exhibit PMA. It should be emphasized, however, for the perfect $L1_2$ structure, where all the three wave-vectors, namely, $\mathbf{q}_1 = (100)$, $\mathbf{q}_2 = (010)$, and $\mathbf{q}_3 = (001)$ contribute, the easy axis is along the [111] direction and the MAE is very small, comparable to that of the disordered alloy. Another [111]-stacked layered structure is generated by $\mathbf{q} = (\frac{1}{2}\frac{1}{2}\frac{1}{2})$ in which there are alternating planes of pure Pt and $\text{Co}_{0.5}\text{Pt}_{0.5}$. In this case also the easy axis is perpendicular to the layer stacking (*i.e.* along [111]) and the MAE is 23.4 μeV . We are not aware of any experimental results on the bulk ordered $\text{Co}_{0.25}\text{Pt}_{0.75}$ system. However, it is reported that [111]-textured thick films grown around 690 K having anisotropic compositional order exhibit large uniaxial anisotropy^{24,25,33} whereas films deposited around 800 K with a $L1_2$ -type isotropic chemical order exhibit no anisotropy. These observations are clearly in good agreement with our results.

The above observations suggest that a large MAE and an easy axis perpendicular to the layer-stacking is a result of existence of in-plane Co-Co bonds and out-of-plane Co-Pt bonds. It has been observed experimentally that in these films there are indeed more Co-Co bonds in-plane and Co-Pt bonds out-of-plane which produce *internal interfaces* analogous to Co/Pt multilayers.³² Be-

cause of the out-of-plane orientation of Co-Pt pairs a hybridization between the Co atoms with large magnetic moment and Pt atoms with strong spin-orbit coupling induces anisotropies in the 3d and 5d orbital moments, the out-of-plane components of the orbital moments become larger than the in-plane components, as has been observed in the x-ray magnetic circular dichroism measurements in the CoPt_3 films.^{26,69} The induced anisotropy in the orbital moments directs the spin moment into a perpendicular alignment through spin-orbit coupling, thus overcoming the in-plane shape anisotropy due to the spin-spin dipole interaction.⁷⁰

B. Magnetic annealing of $\text{Ni}_{0.75}\text{Fe}_{0.25}$ alloy

When $\text{Ni}_{0.75}\text{Fe}_{0.25}$ permalloy is annealed in a magnetic field, an uniaxial magnetic anisotropy is induced depending on the direction of the applied field with respect to the crystallographic axes.^{20,21} This phenomenon, known as magnetic annealing, is interpreted as the creation of directional chemical order in the material.^{45,46} A recent study based on magneto-optic Kerr effect measurements⁷¹ also reveals that magnetic annealing can induce uniaxial anisotropy. Previous studies based on non-relativistic electronic structure calculations⁷² and Monte Carlo simulations⁷³ have shown that in this system compositional and magnetic ordering have a large influence on each other. However, to describe magnetic annealing a fully relativistic treatment is needed. We produce the first quantitative description of magnetic annealing from *ab initio* electronic structure calculations in $\text{Ni}_{0.75}\text{Fe}_{0.25}$. Our results are summarized in Table III. We calculate $S^{(2)}(\mathbf{q}, \mathbf{e})$ for the permalloy in an applied magnetic field of strength 600 Oe (same as used in the experiment²⁰) oriented along $\mathbf{e} = [001]$, [111], and [100] directions of the crystal. We find that when the magnetic field is along [001] (column 2) $S^{(2)}(\mathbf{q})$ is maximum for $\mathbf{q} = (001)$ confirming that ordering is favored along the direction of applied field. In this case, the compositional structure is a layered structure along the [001] direction comprising of alternate pure Ni layers and disordered $\text{Ni}_{0.5}\text{Fe}_{0.5}$ layers. Noting that the measured intensity in a scattering experiment is proportional to the ASRO parameter $\alpha(\mathbf{q})$, we present the ASRO parameters calculated at 722 K (1 K above the ordering temperature) for different \mathbf{q} -vectors in Table IV. We note that when the applied magnetic field is along the [001] direction, $\alpha(\mathbf{q})$ for $\mathbf{q} = (001)$ is 40-50% larger than that at other \mathbf{q} -vectors. Therefore, when the alloy is annealed in the magnetic field, the superlattice spot in the measured intensity at $\mathbf{q} = (001)$ will be 40-50% more intense than that at $\mathbf{q} = (100)$ at a temperature 1 K above the transition temperature. When the magnetic field is applied along the [100] direction, a similar structure perpendicular to [100] direction is favored. However, when the applied field is along [111] direction (column 6) all

the three orderings, namely, (100), (010), and (001) are favored equally. Thus, in this case, we will get a Cu₃Au-type L₁₂ ordering. The calculated transition temperature 721 K is in good agreement with the experimental value⁷⁴ of 820 K.

We have also calculated the MAE of Ni_{0.75}Fe_{0.25} permalloy for different ordered structures. We found that the MAE of the disordered phase is very small (less than 0.1 μeV) and in case of directional chemical ordering it is of the order of μeV, an increase by an order of magnitude. However, in case of perfect ordering, which is L₁₂, the MAE becomes very small as in the disordered phase. This is consistent with experimental observations of Chikazumi²⁰ and Ferguson.²¹

V. ELECTRONIC ORIGIN OF MAGNETIC ANISOTROPY

In elemental solids and the disordered alloys the MAE originates from a redistribution of electronic states around the Fermi level caused by the change in the magnetization direction.³⁸ The electronic structure of the disordered phase around the Fermi level is also partly responsible for the tendency to compositional order in some alloys.^{51,53} The enhancement of MAE in the compositionally modulated alloys is also related to the electronic structure around the Fermi level in the disordered phase. Consequently, to understand the electronic origin of large MAE in the ordered phase, in the following we analyze the Bloch spectral function of the disordered Co_{0.5}Pt_{0.5} alloy along the lines as depicted in Eq. (2.12).

First we consider the ordering tendency. As presented in Table I, our calculation predicts L₁₀-type order in Co_{0.5}Pt_{0.5} which is in excellent agreement with experiment. The quantity $S^{(2)}(\mathbf{q}; \mathbf{e})$ given by Eq. (2.5) can be rewritten as,

$$S^{(2)}(\mathbf{q}; \mathbf{e}) = -\frac{Im}{\pi} \int_{-\infty}^{\infty} d\varepsilon f(\varepsilon, \nu) F(\mathbf{q}, \varepsilon; \mathbf{e})$$

where,

$$F(\mathbf{q}, \varepsilon; \mathbf{e}) = \sum_{L_1 L_2 L_3 L_4} \left[\{X^A(\mathbf{e}) - X^B(\mathbf{e})\}_{L_1 L_2} \times I_{L_2 L_3; L_4 L_1}(\mathbf{q}; \mathbf{e}) \Lambda_{L_3 L_4}(\mathbf{q}; \mathbf{e}) \right]. \quad (5.1)$$

$S^{(2)}(\mathbf{q})$ is an integrated quantity and can also be written in terms of a sum⁷⁵ over Matsubara frequencies,⁷⁶ $\omega_n = (2n + 1)\pi k_B T$,

$$S^{(2)}(\mathbf{q}; \mathbf{e}) = 2k_B T \sum_n Re [F(\mathbf{q}, \nu + i\omega_n; \mathbf{e})].$$

In Fig. 3 we show a plot of $F(\mathbf{q}, \varepsilon; [001])$ calculated for energies along the imaginary axis perpendicular to the

Fermi level for \mathbf{q} -vectors (000), (001), ($\frac{1}{2} \frac{1}{2} \frac{1}{2}$) and ($10\frac{1}{2}$). The area under these curves is indicative of the strength of $S^{(2)}(\mathbf{q}; [001])$ for these \mathbf{q} -vectors and is obviously greatest for $\mathbf{q} = (100)$.

In special cases the electronic structure near the Fermi surface can explain some unusual ordering tendencies. One famous example is a nesting of the Fermi surface^{51,52} which takes place over extended regions of the reciprocal space between almost parallel sheets of Fermi surfaces as in Cu_{0.75}Pd_{0.25} and gives rise to its incommensurate ordering tendency. However, presence of van Hove singularities can give rise to a somewhat different kind of mechanism of ordering in which the spanning vector couples only the regions around two high-symmetry points⁶¹ as in the case of CuPt. In Fig. 4 we show a density-plot of the Bloch spectral density function of the disordered Co_{0.5}Pt_{0.5} alloy in the (001) plane ($k_z = 0$). In this figure the Γ -points are at the corners and the X-points are at the center of the edges. White areas indicate relatively larger density of states. The cross-section of the Fermi surface sheets are seen quite clearly. In this figure we do not observe any van Hove singularities at the symmetry points, the ordering tendency coming instead from states over a wide energy range. However, we do notice that, there are large densities of states around the X-points as well as around the (110) points.

Now we discuss the enhancement of MAE. Again, the quantity $K^{(2)}(\mathbf{q})$ given by Eq. (2.11) is an integrated quantity which can be written as a sum of contributions evaluated at the Matsubara frequencies,⁷⁵

$$K^{(2)}(\mathbf{q}) = 2k_B T \sum_n Re [\Delta F(\mathbf{q}, \nu + i\omega_n)] \quad (5.2)$$

where

$$\Delta F(\mathbf{q}, \varepsilon) = F(\mathbf{q}, \varepsilon; \mathbf{e}_1) - F(\mathbf{q}, \varepsilon; \mathbf{e}_2). \quad (5.3)$$

In Fig. 5 we show a plot of $\Delta F(\mathbf{q}, \varepsilon)$ with $\mathbf{e}_1 = [001]$ and $\mathbf{e}_2 = [111]$ calculated for energies along the imaginary axis perpendicular to the Fermi level for \mathbf{q} -vectors (000), (001), ($\frac{1}{2} \frac{1}{2} \frac{1}{2}$) and ($10\frac{1}{2}$). The area under these curves is indicative of the magnitude of $K^{(2)}(\mathbf{q})$ for these \mathbf{q} -vectors. The striking feature is that the principal contributions are near the real axis indicating that the Fermi surface plays the dominant role in the enhancement of the MAE as well as the direction of easy magnetization. *We propose that such Fermi surface contributions are widespread factors in the enhancement of MAE by compositional order in many magnetic alloys.*

The origin of the enhancement of MAE and the role of the Fermi surface can be easily understood by analyzing the sum and difference of Bloch spectral density functions for the two magnetization directions as outlined in Eq. (2.12). Obviously, we are looking for the spanning vector \mathbf{Q} which connects the high density regions in $\Sigma(\mathbf{q}, \nu)$, the sum of the Bloch spectral density functions for two magnetisation directions, and $\Delta(\mathbf{q}, \nu)$, the difference of the Bloch spectral density functions for two

magnetisation directions, as defined in Eqs. (2.13) and (2.14). In Fig. 6 we show a density-plot of $\Sigma(\mathbf{q}, \nu)$ and $\Delta(\mathbf{q}, \nu)$ of the disordered Co_{0.5}Pt_{0.5} alloy at the Fermi energy in the (010) plane ($k_y = 0$). In this figure the Γ -points are at the corners and the X-points are at the center of the edges. In the density-plot of $\Sigma(\mathbf{q}, \nu)$ the white areas indicate relatively larger values and the most dark areas indicate zero values, whereas in the density-plot of $\Delta(\mathbf{q}, \nu)$ the most white (most dark) areas indicate large positive (negative) values and the grey areas indicate intermediate values. As in case of the Bloch spectral density function, we do not observe large values at the symmetry points. The analysis is more complicated for other \mathbf{q} -vectors but we can conclude that the enhancement of MAE for concentration wave-vectors near the Brillouin zone boundary is indeed due to large values of $\Sigma(\mathbf{q}, \nu)$ and $\Delta(\mathbf{q}, \nu)$ at the Brillouin zone boundary.

Now we discuss the electronic origin of magnetic annealing effect in Ni_{0.75}Fe_{0.25} alloy. We note from Table III that the difference between $S^{(2)}(\mathbf{q}; [001])$ and $S^{(2)}(\mathbf{q}; [100])$ for different \mathbf{q} -vectors is quite small, but as depicted in Table IV it is large enough to be observed by diffuse x-ray, electron and neutron scattering experiments. Because of the small difference in these quantities, in Fig. 7 we plot the real part of $\Delta F(\mathbf{q}, \varepsilon)$ which is related to the difference between $S^{(2)}(\mathbf{q}; [001])$ and $S^{(2)}(\mathbf{q}; [100])$ for $\mathbf{q}=(001)$ for energies along the imaginary axis perpendicular to the Fermi level (left-hand scale). We also plot $F(\mathbf{q}, \varepsilon; [001])$ which is related to $S^{(2)}(\mathbf{q}; [001])$ for $\mathbf{q}=(001)$ for the same energies (right-hand scale). We note that, these two quantities peak near the Fermi energy, i.e. when the imaginary part of the energy is very small. This is an indication that this process is also governed by the electrons near the Fermi surface.

VI. CONCLUSIONS

We have presented the details of our *ab initio* theory of the connection of magnetocrystalline anisotropy of ferromagnetic alloys with the compositional order within the SPR-KKR-CPA scheme. This theory has been applied to fcc-Co_cPt_{1-c} alloys. We found that when cooled from a high temperature, fcc-Co_{0.5}Pt_{0.5} tends to order into $L1_0$ layered-ordered structure around 1360 K and fcc-Co_{0.25}Pt_{0.75} tends to order into $L1_2$ structure around 935 K, in good agreement with experimental observations. Also, we found that in $L1_0$ ordered CoPt the spontaneous magnetization is along the [001] direction which assumes the *c*-axis of the tetragonal structure, in excellent agreement with experiment. The magnitude of the MAE is also close to the experimental value. In some of the other hypothetical layered-ordered structures with same stoichiometry also the magnetic easy axis lies perpendicular to the layer stacking, with the [111]-stacked CuPt-like $L1_1$ structure having the largest MAE. In the $L1_2$ ordered CoPt₃ the magnetic easy axis is along the

[111] direction which is the same as in its disordered counterpart. The MAE is also not very large. However, in case of directional ordering along either of the [100], [010] or [001] direction the easy axis is along the ordering with greatly enhanced MAE. Finally, by analyzing the electronic structure of the disordered alloy near the Fermi energy we have found that the Fermi surface plays the dominant role in the enhancement of MAE. Within the same theoretical framework we have also been able to explain the appearance of directional chemical order in Ni_{0.75}Fe_{0.25} when it is annealed in an applied magnetic field and linked that also to the alloy's Fermi surface. As a last remark, we look forward to future work in which the effects of compositional structure are fully incorporated into micromagnetic modeling of transition metallic materials via *ab initio* electronic structure calculations.

ACKNOWLEDGMENTS

We thank B.L. Gyorffy for many helpful discussions and encouragement. This research is supported by the Engineering and Physical Sciences Research Council (UK), National Science Foundation (USA), and the Training and Mobility of Researchers Network on "Electronic structure calculation of materials properties and processes for industry and basic sciences". We also thank the computing center CSAR at Manchester University as part of the calculations were performed on their Cray T3E machine.

- ¹ L.M. Falicov, D.T. Pierce, S.D. Bader, R. Gronsky, K.H. Hathaway, H.J. Hopster, D.N. Lambeth, S.P. Parkin, G. Prinz, M. Salamon, I.K. Schuller, and R.H. Victora, *J. Mater. Res.* **5**, 1299 (1990).
- ² T. Wakiyama, in *Physics and Engineering Applications of Magnetism*, edited by Y. Ishikawa and N. Miura (Springer-Verlag, Berlin, 1991), p.133.
- ³ B. Heinrich and J.F. Cochran, *Adv. Phys.* **42**, 523 (1993).
- ⁴ M.T. Johnson, P.J.H. Bloemen, F.J.A. den Broeder, and J.J. de Vries, *Rep. Prog. Phys.* **59**, 15409 (1996).
- ⁵ M.H. Kryder, W. Messner, and L.R. Carley, *J. Appl. Phys.* **79**, 4485 (1996).
- ⁶ D.N. Lambeth, E.M.T. Velu, G.H. Bellesis, L.L. Lee, and D.E. Laughlin, *J. Appl. Phys.* **79**, 4496 (1996).
- ⁷ C. Tsan, M.M. Chen, and T. Yogi, *Proc. IEEE* **81**, 1344 (1993).
- ⁸ X. Le Cann, C. Boeglin, B. Carrière, and K. Hricovini, *Phys. Rev. B* **54**, 373 (1996).
- ⁹ H.A. Dürr, G. van der Laan, J. Lee, G. Lauhoff, and J.A.C. Bland, *Science* **277**, 213 (1997).
- ¹⁰ G.H.O. Daalderop, P.J. Kelly, and F.J.A. den Broeder, *Phys. Rev. Lett.* **68**, 682 (1992).
- ¹¹ P. Bruno, *Phys. Rev. B* **39**, 865 (1989).

¹² H. Brooks, Phys. Rev. **58**, B909 (1940).

¹³ H.J.F. Jansen, Phys. Rev. B **38**, 8022 (1988).

¹⁴ G. Hadjipanayis and P. Gaunt, J. Appl. Phys. **50**, 2358 (1979).

¹⁵ B. Zhang and W.A. Soffa, Scr. Metall. Mater. **30**, 683 (1994).

¹⁶ R.A. McCurrie and P. Gaunt, Philos. Mag. **13**, 567 (1966); P. Gaunt, *ibid* 579 (1966).

¹⁷ N. Miyata, K. Tomotsune, H. Nakada, M. Hagiwara, H. Kadomatsu, and H. Fujiwara, J. Phys. Soc. Jpn. **55**, 946 (1986).

¹⁸ N. Miyata, M. Hagiwara, H. Kunitomo, S. Ohishi, Y. Ichiyanagi, K. Kuwahara, K. Tsuru, H. Kadomatsu, and H. Fujiwara, J. Phys. Soc. Jpn. **55**, 953 (1986).

¹⁹ N. Miyata, H. Asami, T. Mizushima, and K. Sato, J. Phys. Soc. Jpn. **59**, 1817 (1990).

²⁰ S. Chikazumi, J. Phys. Soc. Japan. **11**, 551 (1956)

²¹ E.T. Ferguson, J. Appl. Phys. **29**, 252 (1958).

²² D. Weller, H. Brändle, G. Gorman, C.-J. Lin, and H. Notarys, Appl. Phys. Lett. **61**, 2726 (1992)

²³ D. Weller, H. Brändle, and C. Chappert, J. Magn. Magn. Mater. **121**, 461 (1993).

²⁴ M. Maret, M.C. Cadeville, R. Poinsot, A. Herr, E. Beaurepair, and C. Monier, J. Magn. Magn. Mater. **166**, 45 (1997).

²⁵ M. Maret, M.C. Cadeville, W. Staiger, E. Beaurepair, R. Poinsot, and A. Herr, Thin Solid Films **275**, 224 (1996).

²⁶ W. Grange, M. Maret, J.-P. Kappler, J. Vogel, A. Fontaine, F. Petroff, G. Krill, A. Rogalev, J. Goulon, M. Finazzi, and N.B. Brooks, Phys. Rev. B **58**, 6298 (1998).

²⁷ S. Iwata, S. Yamashita, and S. Tsunashima, IEEE Trans. Magn. **MAG-33**, 3670 (1997).

²⁸ S. Iwata, S. Yamashita, and S. Tsunashima, J. Magn. Magn. Mater. **198-199**, 381 (1999).

²⁹ G.R. Harp, D. Weller, T.A. Rabedeau, R.F.C. Farrow, and M.F. Toney, Phys. Rev. Lett. **71**, 2493 (1993).

³⁰ Y. Yamada, T. Suzuki, and E.N. Abarra, IEEE Trans. Magn. **MAG-34**, 343 (1998).

³¹ S. Hashimoto, Y. Ochiai, and K. Aso, J. Appl. Phys. **66**, 4909 (1989).

³² T.A. Tyson, S.D. Conradson, R.F.C. Farrow, and B.A. Jones, Phys. Rev. B **54**, 3702 (1996).

³³ P.W. Rooney, A.L. Shapiro, M.Q. Tran, and F. Hellman, Phys. Rev. Lett. **75**, 1843 (1995).

³⁴ P. Kamp, A. Marty, B. Gilles, R. Hoffmann, S. Marchesini, M. Belakhovsky, C. Boeglin, H.A. Dürr, S.S. Dhesi, G. van der Laan, and A. Rogalev, Phys. Rev. B **59**, 1105 (1999).

³⁵ S.S.A. Razee, J.B. Staunton, B. Ginatempo, F.J. Pinski, and E. Bruno, Phys. Rev. Lett. **83**, 5369 (1999).

³⁶ H. Ebert, B. Drittler, and H. Akai, J. Magn. Magn. Mater. **104-107**, 733 (1992).

³⁷ A.G. Khachaturyan, *Theory of Structural Transformations in Solids* (Wiley, New York, 1983), p.39.

³⁸ S.S.A. Razee, J.B. Staunton, and F.J. Pinski, Phys. Rev. B **56**, 8082 (1997).

³⁹ S.S.A. Razee, J.B. Staunton, F.J. Pinski, B. Ginatempo, and E. Bruno, J. Appl. Phys. **83**, 7097 (1998).

⁴⁰ C.J. Lin and G.L. Gorman, Appl. Phys. Lett. **61**, 1600 (1992).

⁴¹ D. Treves, J.T. Jacobs, and E. Sawatzky, J. Appl. Phys. **46**, 2760 (1975).

⁴² R. Carey, L. Dieu, and D.M. Newman, J. Magn. Magn. Mater. **175**, 99 (1997).

⁴³ P. Poulopoulos, M. Angelakeris, D. Niarchos, and N.K. Flavaris, J. Magn. Magn. Mater. **140-144**, 613 (1995).

⁴⁴ D.M.C. Nicholson, W.H. Butler, W.A. Shelton, Y. Wang, X.-G. Zhang, G.M. Stocks, and J.M. MacLaren, J. Appl. Phys. **81**, 4023 (1997).

⁴⁵ L. Néel, Compt. Rend. **237**, 1613 (1953); J. Phys. Radium **15**, 225 (1954).

⁴⁶ S. Taniguchi, Sci. Rep. Res. Inst. Tohoku Univ. **A 7**, 269 (1955).

⁴⁷ A.H. MacDonald and S. Vosko, J. Phys. C **12**, 2977 (1979).

⁴⁸ A.K. Rajagopal, J. Phys. C **11**, L943 (1978).

⁴⁹ M.V. Ramana and A.K. Rajagopal, Adv. Chem. Phys. **54**, 231 (1983).

⁵⁰ P. Strange, H. Ebert, J.B. Staunton, and B.L. Gyorffy, J. Phys. Condens. Matter **1**, 2959 (1989).

⁵¹ B.L. Gyorffy and G.M. Stocks, Phys. Rev. Lett. **50**, 374 (1983).

⁵² B.L. Gyorffy, D.D. Johnson, F.J. Pinski, D.M. Nicholson, and G.M. Stocks, in *Alloy Phase Stability*, edited by G.M. Stocks and A. Gonis, NATO ASI Series, vol. 163 (Kluwer Academic, Dordrecht, 1987), p. 421.

⁵³ J.B. Staunton, D.D. Johnson, and F.J. Pinski, Phys. Rev. B **50**, 1450 (1994).

⁵⁴ J.B. Staunton, S.S.A. Razee, M.F. Ling, D.D. Johnson, and F.J. Pinski, J. Phys. D **31**, 2355 (1998).

⁵⁵ D.D. Johnson, J.B. Staunton, and F.J. Pinski, Phys. Rev. B **50**, 1473 (1994).

⁵⁶ R. Evans, Adv. Phys. **28**, 143 (1979).

⁵⁷ J.-P. Hansen and I.R. McDonald, *Theory of Simple Liquids*, (Academic, New York, 1976).

⁵⁸ L. Onsager, J. Am. Chem. Soc. **58**, 1468 (1936).

⁵⁹ P. Lloyd, Proc. Phys. Soc. London **90**, 207 (1967).

⁶⁰ J.S. Faulkner and G.M. Stocks, Phys. Rev. B **21**, 3222 (1980).

⁶¹ J.F. Clark, F.J. Pinski, D.D. Johnson, P.A. Stern, J.B. Staunton, and B. Ginatempo, Phys. Rev. Lett. **74**, 3225 (1995).

⁶² R. Zeller, J. Deutz, and P.H. Dederichs, Solid State Commun. **44**, 993 (1982).

⁶³ E. Bruno and B. Ginatempo, Phys. Rev. B **55**, 12946 (1997).

⁶⁴ M. Hansen and K. Anderko, *Constitution of Binary Alloys*, (McGraw-Hill, New York, 1958).

⁶⁵ C. Leroux, M.C. Cadeville, V. Pierron-Bohnes, G. Inden, and F. Hinz, J. Phys. F **18**, 2033 (1988).

⁶⁶ A.A. Aboaf, S.R. Herd, and E. Klokholt, IEEE Trans. Magn. **MAG-19**, 1514 (1983).

⁶⁷ A.J. Freeman, R. Wu, M. Kim, and V.I. Gavrilenko, J. Magn. Magn. Mater. **203**, 1 (1999).

⁶⁸ I.V. Solovyev, P.H. Dederichs, and I. Mertig, Phys. Rev. B **52**, 13419 (1995).

⁶⁹ W. Grange, J.P. Kappler, M. Maret, J. Vogel, A. Fontaine, F. Petroff, G. Krill, A. Rogalev, J. Goulon, M. Finazzi, N. Brookes, J. Appl. Phys. **83**, 6617 (1998).

⁷⁰ D. Weller, J. Stöhr, R. Nakajima, A. Carl, M.G. Samant, C. Chappert, R. Mégy, P. Beauvillain, P. Veillet, and G.A. Held, Phys. Rev. Lett. **75**, 3752 (1995).

⁷¹ F. Schedin, L. Hewitt, P. Morrall, V.N. Petrov, and G. Thornton, J. Magn. Magn. Mater. **198-199**, 555 (1999).

⁷² J.B. Staunton, D.D. Johnson, and B.L. Gyorffy, J. Appl. Phys. **61**, 3693 (1987).

⁷³ M.-Z. Dang and D.G. Rancourt, Phys. Rev. B **53**, 2291 (1996).

⁷⁴ J. Orehotsky, J.B. Sousa, and M.F. Pinheiro, J. Appl. Phys. **53**, 7939 (1982).

⁷⁵ K. Wildberger, P. Lang, R. Zeller, and P.H. Dederichs, Phys. Rev. B **52**, 11502 (1995).

⁷⁶ G.D. Mahan, *Many Particle Physics*, (Plenum, New York, 1981).

TABLE I. Direct correlation function $S^{(2)}(\mathbf{q}; [001])$ for different \mathbf{q} -vectors for $\text{Co}_c\text{Pt}_{1-c}$ alloys (the respective ordered structures are shown in Fig. 1).

c	\mathbf{q}	Structure	$S^{(2)}(\mathbf{q}; [001])$	T_c (K)
			(eV)	
0.5	(000)	Clustering	-1.51	
	(001)	$L1_0$	0.47	1360
	(100)	$L1_0$	0.47	1360
	($\frac{1}{2}\frac{1}{2}\frac{1}{2}$)	$L1_1$	0.29	
	($10\frac{1}{2}$)		0.19	
0.25	(100)	$L1_2$	0.43	935
	(010)	$L1_2$	0.43	935
	(001)	$L1_2$	0.43	935
	($\frac{1}{2}\frac{1}{2}\frac{1}{2}$)		0.22	
	($1\frac{1}{2}0$)	DO_{22}	0.19	
	($\frac{1}{2}01$)	DO_{22}	0.19	

TABLE II. Magnetocrystalline anisotropy energy $K(\mathbf{q})$ for several compositionally modulated $\text{Co}_c\text{Pt}_{1-c}$ alloys characterized by different \mathbf{q} -vectors (the respective ordered structures are shown in Fig. 1). Here $K(\mathbf{q})$ are calculated with respect to the reference system which has the magnetization along the [001] direction (i.e. $\mathbf{e}_1 = [001]$) of the crystal. Thus, when $K(\mathbf{q}) < 0$ the easy axis is along [001] and when $K(\mathbf{q}) > 0$ the easy axis is along \mathbf{e}_2 .

c	\mathbf{q}	Structure	$\mathbf{e}_2 = [111]$	$\mathbf{e}_2 = [100]$	Easy Axis
			$K(\mathbf{q})$ (μeV)	$K(\mathbf{q})$ (μeV)	
0.5	(001)	$L1_0$	-58.6	-105.6	[001]
	(100)	$L1_0$	39.6	105.9	[100]
	($\frac{1}{2}\frac{1}{2}\frac{1}{2}$)	$L1_1$	152.0	0.0	[111]
	($10\frac{1}{2}$)	[001]-Layered	-158.7	-236.5	[001]
	($\frac{1}{2}01$)	[100]-Layered	85.0	236.3	[100]
0.25	(100)	[100]-Layered	30.5	83.6	[100]
	(010)	[010]-Layered	30.5	0.0	-
	(001)	[001]-Layered	-53.0	-83.6	[001]
	($\frac{1}{2}\frac{1}{2}\frac{1}{2}$)	[111]-Layered	23.4	0.0	[111]
	(100),(010),(001)	$L1_2$	8.0	0.0	[111]
	($1\frac{1}{2}0$)		-52.4	0.0	[001]
	($01\frac{1}{2}$)		100.2	152.5	[100]

TABLE III. Direct correlation function $S^{(2)}(\mathbf{q}; \mathbf{e})$ for different \mathbf{q} -vectors for $\text{Ni}_{0.75}\text{Fe}_{0.25}$ alloy (the respective ordered structures are shown in Fig. 1).

\mathbf{q}	$\mathbf{e}=[001]$		$\mathbf{e}=[100]$		$\mathbf{e}=[111]$	
	$S^{(2)}(\mathbf{q})$ (meV)	T_c (K)	$S^{(2)}(\mathbf{q})$ (meV)	T_c (K)	$S^{(2)}(\mathbf{q})$ (meV)	T_c (K)
(100)	330.880		331.158	720.9	330.973	720.5
(010)	330.880		330.880		330.973	720.5
(001)	331.158	720.9	330.880		330.973	720.5
$(\frac{1}{2}\frac{1}{2}\frac{1}{2})$	-99.291		-99.291		-99.475	
$(10\frac{1}{2})$	99.284		99.096		99.222	
$(\frac{1}{2}01)$	99.096		99.285		99.222	

TABLE IV. Atomic short-range order (ASRO) parameter $\alpha(\mathbf{q}; \mathbf{e})$ calculated at temperature 1 K above the ordering temperature 721 K at few high-symmetry \mathbf{q} -vectors for $\text{Ni}_{0.75}\text{Fe}_{0.25}$ alloy (the respective ordered structures are shown in Fig. 1).

\mathbf{q}	$\mathbf{e}=[001]$	$\mathbf{e}=[100]$	$\mathbf{e}=[111]$
(100)	1509.7	2601.4	1756.2
(010)	1509.7	1509.7	1756.2
(001)	2601.4	1509.7	1756.2
$(\frac{1}{2}\frac{1}{2}\frac{1}{2})$	2.3	2.3	2.3
$(10\frac{1}{2})$	4.3	4.3	4.3
$(\frac{1}{2}01)$	4.3	4.3	4.3

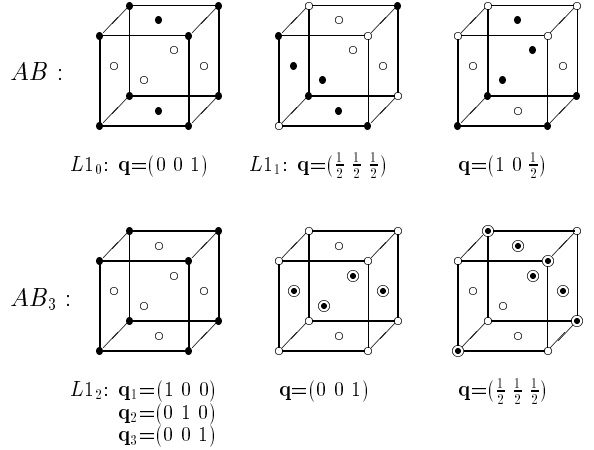


FIG. 1. Some ordered structures and their representative concentration wave-vectors. For the AB -type stoichiometry $\mathbf{q}=(001)$ and $\mathbf{q}=(\frac{1}{2}\frac{1}{2}\frac{1}{2})$ generate respectively the CuAu-type L_{10} layered ordered structure with layers perpendicular to the $[001]$ direction and the CuPt-type L_{11} layered-ordered structure with layers perpendicular to the $[111]$ direction and $\mathbf{q}=(10\frac{1}{2})$ generates a layered structure with planes of an ordered structure of A and B atoms stacked along the $[001]$ direction. For the AB_3 -type composition, a combination of $\mathbf{q}_1=(100)$, $\mathbf{q}_2=(010)$, and $\mathbf{q}_3=(001)$ generates the Cu₃Au-type L_{12} ordered structure. For this composition, a single wave-vector $\mathbf{q}=(001)$ generates a superstructure of alternating monolayers of pure B atoms and disordered $A_{0.5}B_{0.5}$ perpendicular to the $[001]$ direction. Similarly, $\mathbf{q}=(\frac{1}{2}\frac{1}{2}\frac{1}{2})$ generates a superstructure of monolayers of pure B atoms and disordered $A_{0.5}B_{0.5}$ perpendicular to the $[111]$ direction. The full circles denote A atoms, open circles denote B atoms, and a full circle inscribed by an open circle denotes a CPA effective atom $A_{0.5}B_{0.5}$.

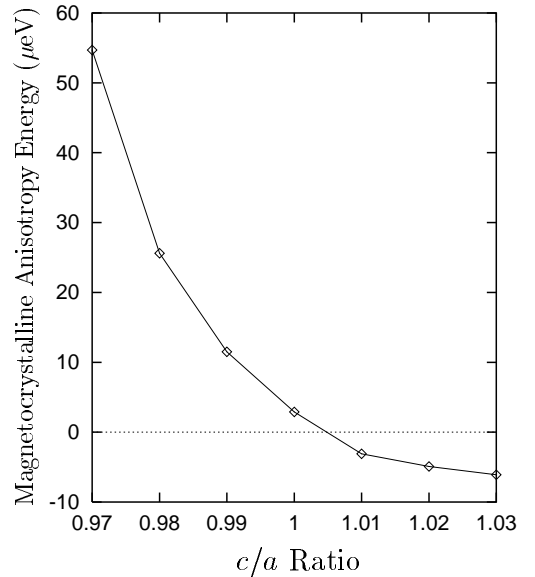


FIG. 2. Magnetocrystalline anisotropy energy (MAE) of disordered volume-conserving face-centered tetragonal (*fct*) $\text{Co}_{0.5}\text{Pt}_{0.5}$ alloy as a function of the c/a ratio.

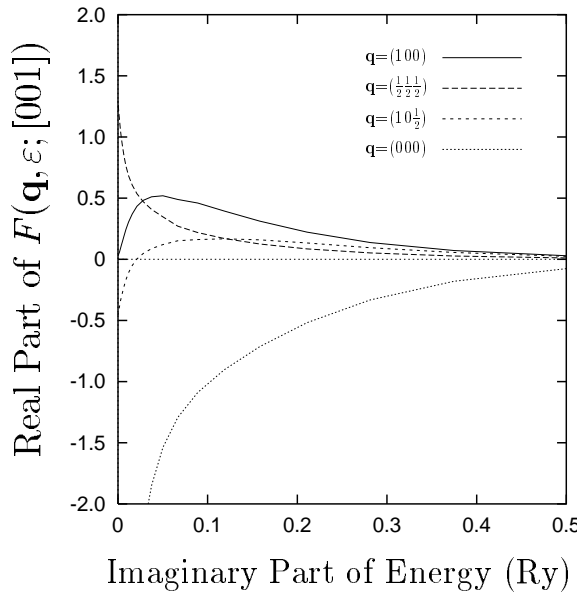


FIG. 3. Real part of $F(\mathbf{q}, \varepsilon, [001])$, as given by Eq. (5.1), for $\mathbf{q}=(100)$ (full line), $(\frac{1}{2}\frac{1}{2}\frac{1}{2})$ (long-dashed line), $(10\frac{1}{2})$ (short-dashed line), and (000) (dotted line) at complex energies along the imaginary axis perpendicular to the Fermi level for disordered $\text{Co}_{0.5}\text{Pt}_{0.5}$ alloy.

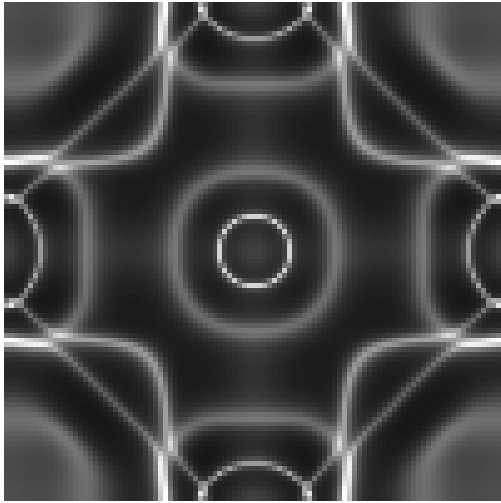


FIG. 4. Density-plot of the Bloch spectral density function of disordered $\text{Co}_{0.5}\text{Pt}_{0.5}$ alloy at the Fermi energy in the (001) plane ($k_z = 0$). The Γ -points are at the corners and the X -points are at the center of the edges. White areas indicate relatively larger density of states.

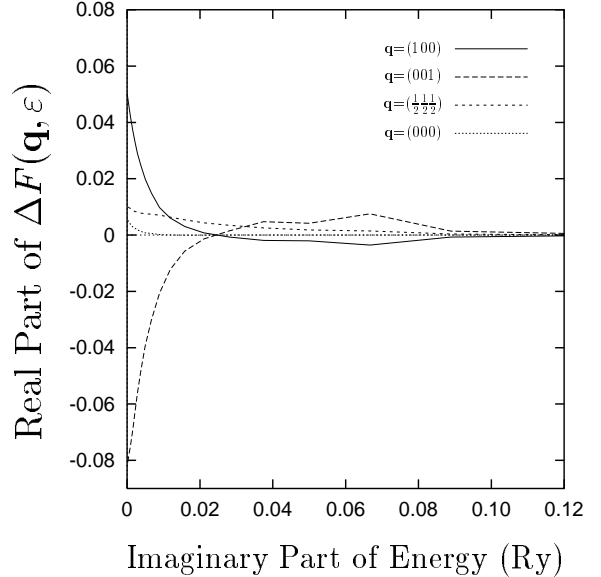


FIG. 5. Real part of $\Delta F(\mathbf{q}, \varepsilon)$, as defined in Eq. (5.3), with $\mathbf{e}_1 = [001]$ and $\mathbf{e}_2 = [111]$ for $\mathbf{q}=(100)$ (full line), (001) (long-dashed line), $(\frac{1}{2}\frac{1}{2}\frac{1}{2})$ (short-dashed line), and (000) (dotted line) at complex energies along the imaginary axis perpendicular to the Fermi level for $\text{Co}_{0.5}\text{Pt}_{0.5}$ alloy. Note the different scales on the y -axes of this figure and Fig. 3.

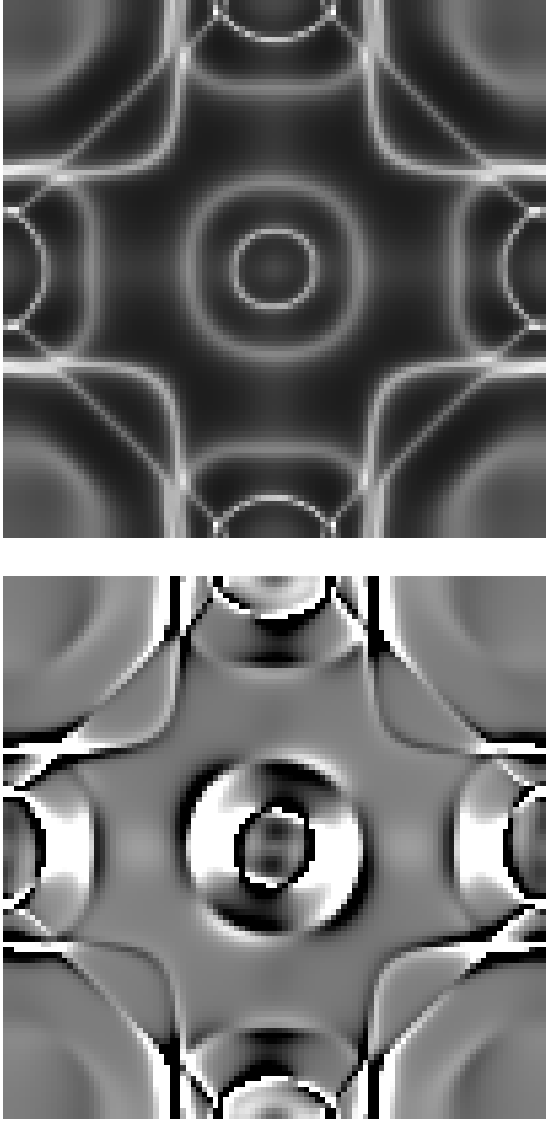


FIG. 6. Density-plot of the sum over two different magnetization directions of the Bloch spectral density functions $\Sigma(\mathbf{q}, \nu)$ (top) and the difference of the Bloch spectral density functions $\Delta(\mathbf{q}, \nu)$ (bottom) as defined in Eqs. (2.13) and (2.14), for disordered $\text{Co}_{0.5}\text{Pt}_{0.5}$ alloy at the Fermi energy in the (010) plane ($k_y = 0$). The Γ -points are at the corners and the X-points are at the center of the edges. White areas indicate relatively larger density of states. In the bottom figure the dark areas indicate negative values rather than zero.

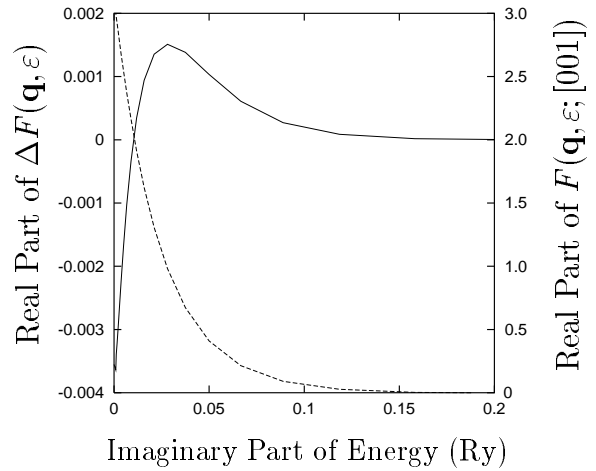


FIG. 7. Real part of $\Delta F(\mathbf{q}, \varepsilon)$ as defined in Eq. (5.3) with $\mathbf{e}_1 = [001]$ and $\mathbf{e}_2 = [100]$ (full line, left scale) and real part of $F(\mathbf{q}, \varepsilon; [001])$, as defined in Eq. (5.1) for $\mathbf{q} = (001)$ (dashed line, right scale) at complex energies along the imaginary axis perpendicular to the Fermi level for $\text{Ni}_{0.75}\text{Fe}_{0.25}$ alloy.